Adaptive Virtual Flux Droop Control Based on Virtual Impedance in Islanded AC Microgrids

Khanabdal, Saheb; Banejad, Mahdi; Blaabjerg, Frede; Hosseinzadeh, Nasser

Published in:
I E E E Journal of Emerging and Selected Topics in Power Electronics

DOI (link to publication from Publisher):
10.1109/JESTPE.2021.3108179

Publication date:
2022

Document Version
Accepted author manuscript, peer reviewed version

Adaptive Virtual Flux Droop Control based on Virtual Impedance in Islanded AC Microgrids

Saheb Khanabdal, Mahdi Banejad, *Senior Member, IEEE,*
Frede Blaabjerg, *Fellow, IEEE,* and Nasser Hosseinzadeh, *Senior Member, IEEE*

Abstract- **Virtual flux droop (VFD) method is a scheme, in which, instead of frequency and voltage amplitude, the phase angle and amplitude of the virtual flux are respectively adjusted to active and reactive power sharing. However, mismatched line impedances lead to improper power sharing. An adaptive virtual flux droop (AVFD) control strategy is proposed in this paper to solve this problem. Firstly, the effect of the mismatched line impedances on the VFD method is analyzed. Then, the idea of virtual impedance is employed to develop the AVFD control strategy. In addition, a small-signal model is presented which is used to tune the control parameters. Furthermore, the microgrid control approach is made based on the direct flux control (DFC) method to apply the proposed strategy. The resultant control scheme is simple without needing multiple feedback loops and complex transformations. In order to validate feasibility and effectiveness of the proposed control strategy, both simulation and experimental studies are implemented. The results show that by the proposed method, accurate power sharing proportional to the ratings of the sources can be achieved in spite of mismatched line impedances.**

***Index Terms*— Power Sharing, Virtual Flux, Droop Control, Microgrid, Virtual Impedance, Inverter, Renewable Energy.**

I. INTRODUCTION

In recent decades, distributed generation (DG) units based on renewable energy sources such as solar arrays and wind turbines have played an important role to address the energy crisis and environmental issues, which can reduce harmful emissions and dependency on fossil fuels [1-4]. In this regard, the concept of microgrid, which is a local power grid including interconnected DGs, storage system units, and loads with coordinated control strategy, has received worldwide attention as a promising approach to facilitate the integration of DGs in the power distribution system. A microgrid can operate in grid-connected or islanded mode. In the first mode, the microgrid is connected to the main grid through the point of common coupling (PCC) and is able to exchange power with the upstream grid. In this condition, the main grid dictates the voltage and frequency due to its higher inertia compared to the microgrid. In the islanded mode, the microgrid operates autonomously. Hence, an effective control strategy, which can keep the power balance between production and consumption as well as maintaining the voltage and the frequency within the desired range, must be applied in this condition.

Inverter based DGs are widely used in the islanded microgrids and are usually connected in parallel. As a result, power supply reliability is improved by providing this redundancy. In such systems, the droop control strategy is a popular method, which can provide the so-called "plug and play" feature for DGs. In spite of the advantages of the droop control method, it suffers from disadvantages including voltage and frequency deviation and dependency on the inverter output impedance [5-6]. In an attempt to solve these issues, several improved strategies based on the droop control method have been proposed which usually use the virtual impedance idea.

The idea of virtual impedance has been investigated in [7-11], which is based on designing and adding virtual resistive, inductive or resistive-inductive impedance into the control loops. Thus, the effects of mismatched output impedances of the inverters are compensated. The resistive-capacitive type of virtual impedance has been introduced to improve the voltage control of the PCC in [12]. However, variations in the parameters of the output filter result in improper reactive power sharing between DGs. A genetic algorithm can be used to calculate the optimized virtual impedance [13], but knowledge of the line parameters is needed. An improved method has been presented in [14], in which the virtual impedance is used in both frequency and voltage control loops. Moreover, the control coefficients are optimized using intelligent algorithms such as particle swarm optimization. However, the number of control coefficients has significantly increased. The multiple control coefficients and the necessity of careful selection of their values lead to the complexity of the control system.

An efficient way of enhancing the virtual flux idea is to establish the communication between DGs together or between DGs and the central control unit in order to send and receive control signals and measured data, as it is used in [8],

Manuscript received XXXX XX, XXXX; revised XXX XX, XXXX and XXXX XX, XXXX; accepted XXXX XX, XXXX. Date of publication XXX XX, XXXX; date of current version XXX XX, XXXX. *(Corresponding author: Mahdi Banejad.)*

S. Khanabdal and M. Banejad are with the Faculty of Electrical Engineering, Shahrood University of Technology, Shahrood 3619995161, Iran (e-mail: khanabdal@shahroodut.ac.ir; m.banejad@shahroodut.ac.ir).

F. Blaabjerg is with the Department of Energy Technology, Aalborg University, 9220 Aalborg, Denmark; (e-mail: fbl@energy.aau.dk)

N. Hosseinzadeh is with the Centre for Smart Power and Energy Research, School of Engineering, Faculty of Science, Engineering and Built Environment, Deakin University, Vic 3216, Australia; (e-mail: nasser.hosseinzadeh@deakin.edu.au)

Color versions of one or more figures in this article are available at https://doi.org/XX.XXXX/JESTPE.XXXX.XXXXXXXX.

Digital Object Identifier XX.XXXX/JESTPE.XXXX.XXXXXXXX.

[15-18]. For example, [15] has developed an adaptive virtual impedance method, which requires low band communication links to adjust the virtual impedance. Therefore, the adverse effects of the output impedance mismatches of inverters are mitigated and appropriate reactive power sharing is achieved. However, voltage regulation cannot be guaranteed and frequency deviations cannot be avoided due to the use of $P-\omega$ droop. Moreover, the use of sinusoidal pulse width modulation (SPWM) technique and complex transformations and the existence of multiple control loops make it difficult to implement it in practice [19].

Improvement in the performance of the frequency loop has received less attention according to the literature. An improved method, in this regard, is the indirect control of the frequency using $P-\delta$ droop, thus allowing for more precise frequency control [20-22]. However, it suffers from some drawbacks such as adjusting an initial value of δ and reactive power sharing errors. The problem of adjusting the initial δ can be solved by using GPS for synchronization. Moreover, the VFD control method has been developed to tackle the issue of improper reactive power sharing, which has a simple control structure and does not require the SPWM to generate the switching signal commands [19]. However, the accuracy of power sharing is severely affected by the unequal line impedances of the inverters.

This paper deals with the adverse impacts of the mismatched line impedances on the accuracy of the VFD control method, which may result in improper power sharing. The main contribution of this paper is proposing an adaptive virtual flux droop control strategy which employs the idea of virtual impedance to mitigate the effects of the mismatched line impedances. Thus, the simple structure of the VFD control method and the effectiveness of the virtual impedance idea are combined which leads to the appropriate power sharing between DGs proportional to their ratings. In addition, a small-signal model is developed to tune the control parameters. Furthermore, the proposed microgrid control scheme is adopted, which employs the direct flux control algorithm to generate the switching signals of the inverters based on the proposed AVFD control strategy. A communication link is used to synchronize and tune the reference active and reactive powers. The merits of the proposed control scheme are:

1) It is straightforward, and it does not require complex transformations.
2) There is no need to use the multiple feedback loops and cascaded control structure of the voltage and current.
3) The knowledge of the line impedance and load is not required to adjust the control parameters. Therefore, there is no need for estimation methods.
4) Appropriate power sharing between inverter based-DGs proportional to their ratings can be achieved in spite of the line impedances being unequal.

The rest of this paper is organized as follows. The virtual flux droop control is described by the mathematical equations in Section II. Then, the proposed control scheme is developed and explained in detail in Section III. Afterward, a small-signal model is presented in section IV, which is used to investigate the stability and adjust the control parameters. In Section V, it is explained how the proposed control scheme is incorporated into the overall control strategy of the microgrid. Section VI provides simulation and experimental laboratory studies to validate the proposed strategy; then, compares and discusses the results obtained by the proposed AVFD strategy versus the conventional VFD. Finally, the paper is summarized in Section VII.

II. Virtual Flux Droop Control Method

A. Motivations

The conventional droop control, which is based on $P-\omega$ and $Q-V$, suffers from poor reactive power sharing. In addition, the voltage and the frequency deviations are inevitable. Moreover, multiple control loops are needed to regulate the voltage and the control accuracy depends on the quality of the inner current control strategy. Furthermore, multiple signal feedbacks, PI regulators and complex coordinate transformation result in a complicated control structure which needs much tuning effort to guarantee stability and good dynamic response.

In the VFD control method, good dynamic and steady-state performance can be achieved by regulating the flux vector. Therefore, it is useful to develop the power sharing scheme based on the flux vector. The resultant control structure is straightforward, as the switching signals are generated by direct control of two independent parameters, while there is no need for the complex transformations, the multiple feedback controls are avoided and the related PI regulators are not required [19]. Furthermore, fast dynamic response, good voltage control and lower frequency deviation as well as proportionally power sharing are provided. However, the mismatched line impedances lead to improper power sharing. The concept of virtual impedance is a popular method to deal with this problem. Nevertheless, because of the simple structure of the VFD control method, it cannot be employed directly. Thus, incorporating the virtual impedance in the structure of the VFD control method is challenging.

Considering the drawbacks of the conventional droop control and VFD control methods, this paper proposes a strategy to overcome these challenges. Firstly, the effects of the virtual impedance on the control parameters of the VFD method are calculated and then the controllers which can produce the same effects are proposed. As a result, the disadvantage of the VFD control method in the case of mismatched line impedances is overcome by using the concept of virtual impedance.

B. Mathematical Equations

Based on [19], a simple islanded microgrid, which consists of two parallel inverter-based DGs is shown in Fig. 1. Each inverter is connected to the PCC through a cable, with the given impedances. This equivalent circuit can be described by:

$$V_i = R_i I_i + L_i \frac{dI_i}{dt} + E \quad (i = 1,2) \tag{1}$$

This article has been accepted for publication in a future issue of this journal, but has not been fully edited. Content may change prior to final publication. Citation information: DOI 10.1109/JESTPE.2021.3108179, IEEE Journal of Emerging and Selected Topics in Power Electronics

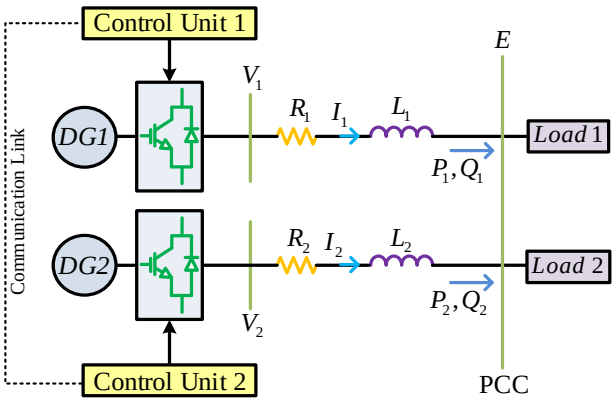

Fig. 1. Simplified model of an islanded microgrid with parallel configuration.

where E is the voltage of the PCC, V_i is the output voltage of inverter i and I_i is its line current. In addition, R_i and L_i are the line resistance and inductance, respectively, connected to DG_i.

As flux can be obtained by the time integral of voltage in electrical machines, the virtual flux vectors are defined as:

$$\psi_i = \int V_i \, dt = \frac{|V_i|}{\omega} e^{j\varphi_i} \tag{2}$$

$$\psi_E = \int E \, dt = \frac{|E|}{\omega} e^{j\varphi_E} \tag{3}$$

where ψ_i and ψ_E are the virtual flux vectors of inverter i and the PCC, respectively. Moreover, φ_i and φ_E are their corresponding angles. Thus, the mathematical equations of the virtual flux droop control for inverter i can be derived as [19]:

$$\bar{\delta}_i = \delta_i^n - m_i \left(P_i^n - P_i \right) \tag{4}$$

$$|\bar{\psi}_i| = |\psi_i^n| - n_i \left(Q_i^n - Q_i \right) \tag{5}$$

where $\delta_i = \varphi_i - \varphi_E$ is the angular difference, P_i^n is the nominal active power and Q_i^n is the nominal reactive power. Moreover, δ_i^n and $|\psi_i^n|$ are the nominal angular difference and amplitude of the virtual flux vector, respectively. Furthermore, m_i and n_i are the droop coefficients. The fundamental power components including P_i and Q_i are extracted by filtering the total active and reactive powers to the PCC. Then, the set values, i.e. $\bar{\delta}_i$ and $|\bar{\psi}_i|$ are specified using the VFD control method.

III. Proposed Control Strategy

Effectiveness of the VFD control method depends on the line impedances. In other words, proportional power sharing will be feasible, if the line impedances are equal. However, the line impedance mismatches deteriorate significantly the effectiveness of the VFD control method and lead to active and reactive power sharing errors. Therefore, it is important to analyze the effect of the line impedance mismatch on the power sharing based on the VFD.

According to Fig. 1, the voltage drop across line i is calculated as:

$$\Delta V_i = V_i - E = Z_i \times I_i \tag{6}$$

And the injected current of inverter i to the PCC is obtained as:

$$I_i = \frac{P_i - jQ_i}{E} \tag{7}$$

Considering $Z_i = R_i + j\omega L_i$ and substituting I_i from (7) in (6) leads to:

$$\Delta V_i = \frac{L_i \omega Q_i + R_i P_i}{E} + j \frac{L_i \omega P_i - R_i Q_i}{E} \tag{8}$$

The angular difference between V_i and E, i.e. θ, is generally small. So, it is supposed that $\sin(\theta) \approx \theta$ and $\cos(\theta) \approx 1$ [15], [19]. Consequently:

$$|\Delta V_i| \simeq |V_i| - |E| \simeq \frac{L_i \omega Q_i + R_i P_i}{E} \tag{9}$$

$$\theta \simeq \frac{L_i \omega P_i - R_i Q_i}{E} \tag{10}$$

which result in:

$$\Delta\psi = |\psi_i| - |\psi_E| \approx \frac{|\Delta V_i|}{\omega} \simeq \frac{|V_i| - |E|}{\omega} \simeq \frac{L_i \omega Q_i + R_i P_i}{E\omega} \tag{11}$$

$$\delta_i = \varphi_i - \varphi_E \simeq \frac{L_i \omega P_i - R_i Q_i}{E} \tag{12}$$

The above equations indicate the effects of the line impedances on the parameters of the VFD control method. Without loss of generality, a microgrid with two DGs, as shown in Fig. 1 is considered and it is assumed that both DGs have the same power ratings. Therefore, each of the DGs should deliver equal active and reactive powers to the PCC. In order to have an equal power sharing for both DGs, the set values for both DGs, i.e. $\bar{\delta}_i$ and $|\bar{\psi}_i|$, have to be equal based on (2)-(3). The parameters of line impedance 2 are considered as references. Therefore:

$$R_2 = R_{ref} \quad , \quad X_2 = X_{ref} \tag{13}$$

The mismatches in the parameters of the line impedances are calculated as:

$$\Delta X = X_1 - X_2 \tag{14}$$

$$\Delta R = R_1 - R_2 \tag{15}$$

Considering (13)-(15), the parameters of the line impedance 1 can be expressed as:

$$X_1 = X_{ref} + \Delta X \tag{16}$$

$$R_1 = R_{ref} + \Delta R \tag{17}$$

Now, the effects of the line impedances on the difference between the virtual flux vectors of the inverters and the PCC can be obtained as follows:

$$\Delta\psi_2 = \Delta\psi_{ref} = \frac{X_{ref} Q_2 + R_{ref} P_2}{E\omega} \tag{18}$$

$$\Delta\psi_1 = \frac{X_{ref} Q_1 + R_{ref} P_1}{E\omega} + \frac{\Delta X Q_1 + \Delta R P_1}{E\omega} = \Delta\psi_{ref} + d\Psi \tag{19}$$

As can be seen from (19), since $\Delta\psi_2 = \Delta\psi_{ref}$, $d\Psi$ is responsible for improper reactive power sharing between the DGs. In a similar manner, the effects of the line impedances on the angular difference can be calculated as follows:

$$\delta_2 = \frac{X_{ref}P_2 - R_{ref}Q_2}{E} \tag{20}$$

$$\delta_1 = \frac{\left(X_{ref} + \Delta X\right)P_1 - \left(R_{ref} + \Delta R\right)Q_1}{E} = \delta_{ref} + d\delta \tag{21}$$

Similarly, $d\delta$ is responsible for improper active power sharing between the DGs. Equal line resistances ($R_1 = R_2$) and equal line reactances $(X_1 = X_2)$ result in $d\Psi = 0$ and $d\delta = 0$. Consequently, accurate power sharing between the sources proportional to their ratings is achieved. But, in the case of the mismatched line impedances, i.e. $(R_1 \neq R_2)$ and $(X_1 \neq X_2)$, $d\Psi$ and $d\delta$ are nonzero, which leads to power sharing errors. In order to deal with this problem, the concept of virtual impedance is a useful approach, which can be employed as:

$$X_V = -\Delta X \tag{22}$$

$$R_V = -\Delta R \tag{23}$$

where X_V and R_V are the virtual reactance and resistance, respectively. Hence, the terms of $d\Psi$ and $d\delta$ in (19) and (21) are mitigated, and therefore the appropriate power sharing between the sources can be achieved. Nevertheless, knowledge of the line impedances, (which are not readily accessible), is required. However, this problem can be resolved by another solution so that the virtual impedance is employed to compensate for the unsuitable effects of the line impedance mismatches on the angular difference and the difference between the fluxes of the inverter and the PCC. The set values for both sources with the same ratings using the VFD control are obtained as:

$$\bar{\delta}_1 = \delta_{ref} + d\delta \tag{24}$$

$$\bar{\delta}_2 = \delta_{ref} \tag{25}$$

$$\left|\bar{\psi}_1\right| = \left|\psi_E\right| + \Delta\psi_{ref} + d\Psi \tag{26}$$

$$\left|\bar{\psi}_2\right| = \left|\psi_E\right| + \Delta\psi_{ref} \tag{27}$$

The set values generated by the VFD should be modified to overcome the unsuitable effects of the line impedance mismatches on the power sharing. The values are:

$$\bar{\delta}_1 + \overline{d\delta} = \delta_{ref} + d\delta \tag{28}$$

$$\left|\bar{\psi}_1\right| + \overline{d\psi} = \left|\psi_E\right| + \Delta\psi_{ref} + d\Psi \tag{29}$$

To meet the above requirements and considering Fig. 2, the control scheme should be designed in such a way:

$$\overline{d\delta} = d\delta \tag{30}$$

$$\overline{d\psi} = d\Psi \tag{31}$$

Hence, the compensatory terms should be added to alleviate $d\Psi$ and $d\delta$. As the knowledge of the line parameters is not readily accessed, matching the impedances is not the aim of this paper. For this reason, the virtual impedance is used as:

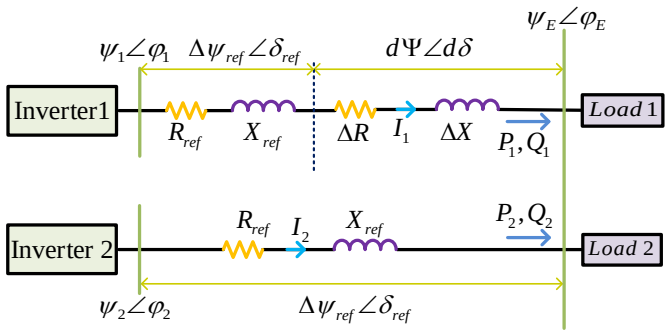

Fig. 2. Simplified structure of microgrid seen from inverter 2.

$$-d\delta_v = \overline{d\delta} \tag{32}$$

$$-d\psi_v = \overline{d\psi} \tag{33}$$

where $d\delta_v$ and $d\psi_v$ are the angular difference and the difference between fluxes of the inverter and the PCC caused by the proposed virtual impedance. Thus:

$$-\frac{X_vP_1 - R_vQ_1}{E\omega} = \frac{\Delta XP_1 - \Delta RQ_1}{E\omega} \tag{34}$$

$$-\frac{X_vP_1 + R_vQ_1}{E\omega} = \frac{\Delta XP_1 + \Delta RQ_1}{E\omega} \tag{35}$$

Finally, this paper suggests using the benefits of the VFD control method and virtual impedance idea simultaneously. Therefore, the adaptive virtual flux droop control strategy, as shown in Fig. 3, is proposed as:

$$\bar{\delta}_i = \delta_i^n - m_i\left(P_i^n - P_i\right) - k_{ip}\int\left(P_i - P^*\right)dt \tag{36}$$

$$\left|\bar{\psi}_i\right| = \left|\psi_i^n\right| - n_i\left(Q_i^n - Q_i\right) - k_{iq}\int\left(Q_i - Q^*\right)dt \tag{37}$$

where k_{ip} and k_{iq} are the compensatory coefficients for active and reactive powers, respectively. The last terms in (36) and (37) produce effects similar to the parameters of the virtual impedance on the set values to compensate for the bad effects of the mismatched line impedances. Thus, the idea of virtual impedance is indirectly employed as mentioned in (32)-(35), while there is no need for the knowledge of the line impedances. As shown in Fig. 3, the simple integral control loops are added to regulate the active and reactive powers. It should be noted that, instead of matching the parameters of the line impedances, the effects of the mismatched line impedances are indirectly compensated. In other words, regarding (34) and (35), the compensatory terms of (36) and (37) produce the same effects as the parameters of the supposed virtual impedance. Therefore, accurate power sharing proportional to the ratings of the sources is achieved.

It should be noted that the data of the power delivered to the PCC by each inverter are transferred to the Energy Management System (EMS) via the communication links and appropriate P^* and Q^* references are sent back to the control units proportional to the ratings of sources, so that, the sources with the same ratings receive the same references. As the communication link is not used in the closed loop control, the accuracy of power sharing is not affected by time delays.

This article has been accepted for publication in a future issue of this journal, but has not been fully edited. Content may change prior to final publication. Citation information: DOI 10.1109/JESTPE.2021.3108179, IEEE Journal of Emerging and Selected Topics in Power Electronics

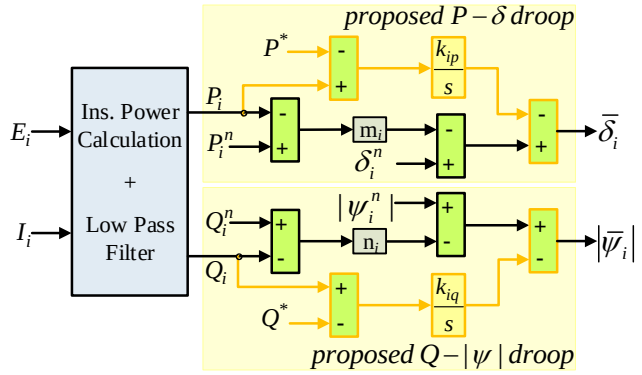

Fig. 3. Proposed adaptive virtual flux droop control.

IV. Small-Signal Analysis

As shown in Fig. 1, DG units are connected to the PCC via power electronic converters. This results in lower inertia compared to the synchronous machines of similar ratings, and therefore dynamic responses are much faster than conventional rotary generators. On the other hand, disturbances can lead to improper power sharing. To address these issues, small-signal analysis is now discussed to investigate the stability of the proposed AVFD control strategy, which can be employed to adjust the control parameters.

The linearized models of the active and reactive powers delivered by each inverter to the PCC [19] are given below:

$$\Delta P(s) = G_p.\Delta\bar{\delta}(s) \tag{38}$$

$$\Delta Q(s) = G_q.\Delta|\bar{\psi}|(s) \tag{39}$$

where Δ represents perturbation values. G_p and G_q are calculated around the operating point and obtained as:

$$G_p = \frac{\omega}{L}|\psi_E||\psi_V|\cos\delta \tag{40}$$

$$G_q = \frac{\omega}{L}|\psi_E|\cos\delta \tag{41}$$

The small-signal dynamics of the proposed AVFD control strategy can be expressed by linearizing (36)-(37) as:

$$\Delta\bar{\delta}(s) = \Delta\delta^n(s) - m\left(\Delta P^n(s) - \frac{\omega_c}{s+\omega_c}\Delta P(s)\right) - \frac{k_p}{s}\left(\frac{\omega_c}{s+\omega_c}\Delta P(s) - \Delta P^*(s)\right) \tag{42}$$

$$\Delta|\bar{\psi}|(s) = \Delta|\psi^n|(s) - n\left(\Delta Q^n(s) - \frac{\omega_c}{s+\omega_c}\Delta Q(s)\right) - \frac{k_q}{s}\left(\frac{\omega_c}{s+\omega_c}\Delta Q(s) - \Delta Q^*(s)\right) \tag{43}$$

where the low pass filter can be modeled as a first order approximation, in which ω_c is the cut-off angular frequency. Considering ΔP as the output and $\Delta\delta^n$, ΔP^n and ΔP^* as the inputs of the $P-\delta$ droop control loop, it is achieved that:

$$\Delta P(s) = \frac{G_p(s+\omega_c)}{denP}\left(s\left(\Delta\delta^n(s) - m\Delta P^n(s)\right) + k_p\Delta P^*(s)\right) \tag{44}$$

Accordingly, the characteristic equation of (44) is obtained as:

$$denP:\ s^2 + \omega_c(1-G_p m)s + k_p\omega_c G_p = 0 \tag{45}$$

Similarly, considering ΔQ as the output and $\Delta|\psi^n|$, ΔQ^n and ΔQ^* as the inputs of the $Q-|\psi|$ droop control loop, it is obtained that:

$$\Delta Q(s) = \frac{G_q(s+\omega_c)}{denQ}\left(s\left(\Delta|\psi^n|(s) - n\Delta Q^n(s)\right) + k_q\Delta Q^*(s)\right) \tag{46}$$

Subsequently, the related characteristic equation is derived as:

$$denQ:\ s^2 + \omega_c(1-G_q n)s + k_q\omega_c G_q = 0 \tag{47}$$

The eigenvalues of the characteristic equations (45) and (47) are related to the parameters of the proposed control scheme, which should be adjusted to ensure system stability. In this regard, the trajectories of the eigenvalues related to (44) with respect to change k_p and L_{eq} for both simulation and experimental parameters are shown in Fig. 4. Furthermore, Fig. 5 shows the trajectories of the eigenvalues corresponded to (47) with respect to change k_q and L_{eq} for both simulation and experimental parameters. The eigenvalues of $P-\delta$ and $Q-|\psi|$ control loops are on the left side of the imaginary axis for $k_p > 0$ and $k_q > 0$, respectively. Moreover, as the equivalent inductance of line and filter, i.e. L_{eq}, increases, the eigenvalues get closer to the imaginary axis from the left. In addition, because of the conflict between the maximum overshoot and the rise time in typical second order models, the damping ratio should be between 0.4 and 0.8 [22-23]. Considering this constraint for (45) and (47) leads that:

$$0.4 \le \frac{\omega_c(1-G_p m)}{2\times\sqrt{k_p\omega_c G_p}} \le 0.8 \tag{48}$$

$$0.4 \le \frac{\omega_c(1-G_q n)}{2\times\sqrt{k_q\omega_c G_q}} \le 0.8 \tag{49}$$

As a result, the transient response will be adequately fast and be sufficiently damped [23]. The permissible ranges of k_p and k_q to establish (48) and (49) are obtained as:

$$\frac{\omega_c(1-G_p m)^2}{1.6^2 G_p} \le k_p \le \frac{\omega_c(1-G_p m)^2}{0.8^2 G_p} \tag{50}$$

$$\frac{\omega_c(1-G_q n)^2}{1.6^2 G_q} \le k_q \le \frac{\omega_c(1-G_q n)^2}{0.8^2 G_q} \tag{51}$$

As $G_p > 0$, $G_q > 0$, $m < 0$, $n < 0$ and $\omega_c > 0$, therefore:

$$0 < \frac{\omega_c(1-G_p m)^2}{1.6^2 G_p} \tag{52}$$

$$0 < \frac{\omega_c(1-G_q n)^2}{1.6^2 G_q} \tag{53}$$

Regarding (50)-(53), the final design ranges of permissible values for k_p and k_q are respectively equal to (50) and (51)

This article has been accepted for publication in a future issue of this journal, but has not been fully edited. Content may change prior to final publication. Citation information: DOI 10.1109/JESTPE.2021.3108179, IEEE Journal of Emerging and Selected Topics in Power Electronics

which satisfy the stability and appropriate transient response criteria, simultaneously.

In the following, the effects of the communication delay on the transient response behavior of the system are investigated. As mentioned previously, the control parameters are tuned based on the small-signal analysis. In fact, the values of these parameters are adjusted offline for each inverter using its corresponding local data, while there is no need to communicate with the EMS. Furthermore, until the load is not changed, the reference values of P^* and Q^* will not change, and therefore in this condition, the accuracy of the power sharing is not affected by the communication time delays. Nevertheless, in order to theoretically study the effects of the communication time delay on the dynamic behavior of the proposed control strategy, small-signal analysis is carried out. Regarding that τ_D is the time delay in the communication links, (42) and (43) are changed as:

$$\begin{aligned}\Delta\bar{\delta}(s)=\Delta\delta^n(s)-m\left(\Delta P^n(s)-\frac{\omega_c}{s+\omega_c}\Delta P(s)\right)\\-\frac{k_p}{s}\left(\frac{\omega_c}{s+\omega_c}\Delta P(s)-\frac{1}{\tau_D s+1}\Delta P^*(s)\right)\end{aligned}\tag{54}$$

$$\begin{aligned}\Delta|\bar{\psi}|(s)=\Delta|\psi^n|(s)-n\left(\Delta Q^n(s)-\frac{\omega_c}{s+\omega_c}\Delta Q(s)\right)\\-\frac{k_q}{s}\left(\frac{\omega_c}{s+\omega_c}\Delta Q(s)-\frac{1}{\tau_D s+1}\Delta Q^*(s)\right)\end{aligned}\tag{55}$$

In a similar manner to reach (45) and (47), the characteristic equations of $P-\delta$ and $Q-|\psi|$ control loops by considering the communication delay are respectively obtained as:

$$\underbrace{(s^2+\omega_c(1-G_p m)s+k_p\omega_c G_p)}_{A1}\underbrace{(\tau_D s+1)}_{B}=0\tag{56}$$

$$\underbrace{(s^2+\omega_c(1-G_q n)s+k_q\omega_c G_q)}_{A2}\underbrace{(\tau_D s+1)}_{B}=0\tag{57}$$

Based on the above characteristic equations, the responses of $P-\delta$ and $Q-|\psi|$ control loops in the proposed control strategy are the sum of the first order (B) and the second order ($A1$ and $A2$) systems [23]. Furthermore, $A1$ and $A2$ are the characteristic equations achieved in (45) and (47), respectively. Although the root of the first order equation only relies on the time delay, the roots of the second order equations are independent from the time delay and are only affected by the control parameters. A necessary condition to fulfill (48) is that the roots of $A1$ have to be complex-conjugate. Similarly, this point has to be established for $A2$ to satisfy (49). Moreover, in order to lessen the communication time delay impacts on the transient response, the control parameters are selected such that the absolute values of the real parts of the roots of $A1$ and $A2$, i.e. σ_{A1} and σ_{A2} should meet the following criteria:

$$\sigma_{A1}\le 0.2\tau_D^{-1}\tag{58}$$

$$\sigma_{A2}\le 0.2\tau_D^{-1}\tag{59}$$

Satisfying (58) and (59) means that the ratios between the absolute value of the real part of the pole which is made by the time delay, i.e. $1/\tau_D$, and the absolute values of the real parts of the poles belong to the second order equations, i.e. σ_{A1} and σ_{A2} exceed 5. Therefore, the roots of $A1$ and $A2$ become the dominant poles for $P-\delta$ and $Q-|\psi|$ control loops,

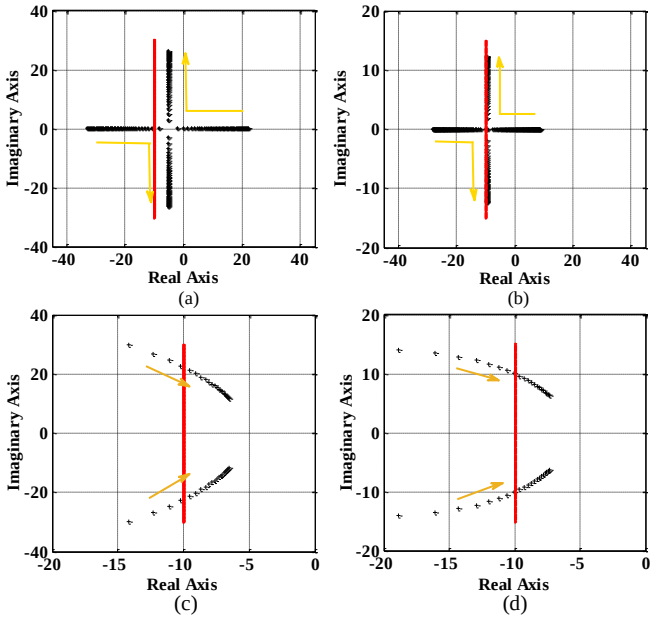

Fig. 4. The trajectory of closed loop poles of $P-\delta$ droop control:
(a) with respect to change k_p based on simulation parameters.
(b) with respect to change k_p based on experimental parameters.
(c) with respect to change L_{eq} based on simulation parameters.
(d) with respect to change L_{eq} based on experimental parameters.

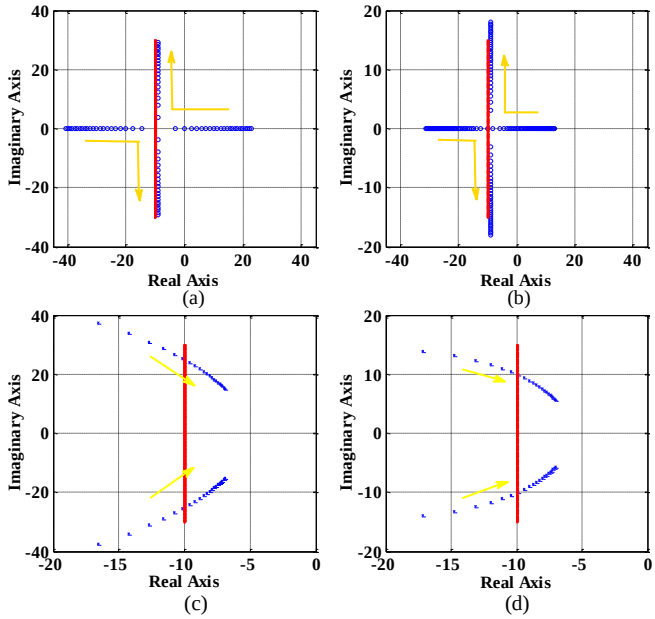

Fig. 5. The trajectory of closed loop poles of $Q-|\psi|$ droop control:
(a) with respect to change k_q based on simulation parameters.
(b) with respect to change k_q based on experimental parameters.
(c) with respect to change L_{eq} based on simulation parameters.
(d) with respect to change L_{eq} based on experimental parameters.

respectively. As a result, the transient response behavior of the system is only affected by the control parameters and immunes from the communication delay. Here, the maximum time delay is considered 20 ms. Therefore, the pole of B in (56) and (57) is located in $s=-1/\tau_D=-50$. Based on (58) and (59), the line $\sigma=-1/(5\tau_D)=-10$ is plotted by a red vertical line in Figs. (4) and (5). Thus the operating points for $P-\delta$ and $Q-|\psi|$ control loops in the proposed control strategy have to be between the mentioned red line and the imaginary axis. As can be seen, it is completely possible to simultaneously satisfy (58) and (48) for $P-\delta$ control loop and also (59) and (49) for $Q-|\psi|$ control loop. Therefore, the time delays less than 20 ms do not impact on the transient response in this paper. It is worth mentioning that the parameters of the control system can be adjusted in such a way that the larger values of the time delay will not adversely affect the transient response of the system. However, it leads to slower transient response.

V. Proposed Microgrid Control Strategy

The proposed microgrid control scheme is shown in Fig. 6, where the AVFD control strategy is used to compute the command signals i.e. the angular difference and the virtual flux amplitude for each inverter and accordingly, DFC is employed to generate the appropriate switching vector. Thus, both control quantities are compared to their respective instantaneous values, which are calculated using the current voltage vector. The generated errors are the inputs of the hysteresis controllers. A three-level controller is used for the angular difference error and a two-level controller is employed for the virtual flux amplitude error. Furthermore, the $\alpha-\beta$ plane is divided into six sections, as shown in Fig. 7, where two null and six active voltage vectors are also depicted, and the number of the sector, where the virtual flux vector of the inverter is located, is specified. Finally, the appropriate voltage vector, which should be applied to the inverter, is selected based on the basic idea of the DFC strategy from Table I, where m is the sector number, ε_δ and ε_ψ are the outputs of angular difference and virtual flux hysteresis controllers, respectively.

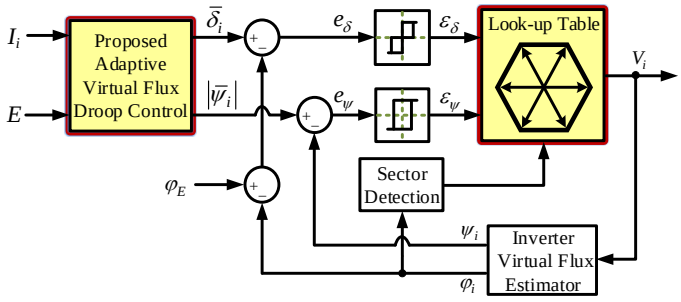

Fig. 6. Block diagram of the proposed microgrid control strategy.

TABLE I
SWITCHING TABLE OF DFC STRATEGY

ε_δ	ε_ψ	Selected voltage
1	1	V_{m+1}
1	0	V_{m+2}
0	1	V_0
0	0	V_0
-1	1	V_{m+5}
-1	0	V_{m+4}

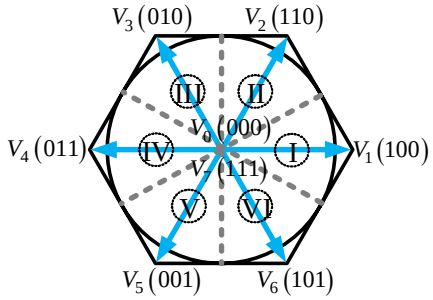

Fig. 7. Voltage space vectors in the $\alpha-\beta$ plane.

It should be noted that the frequency and the voltage amplitude of the PCC are controlled indirectly. In other words, firstly, a three-phase AC voltage with a constant frequency defined as a virtual reference is employed to compute the angle of the virtual flux vector of the PCC. Then, it is subtracted from the angle of the virtual flux vector of the inverter, and therefore the instantaneous angular difference is obtained. As it is controlled firmly, both virtual flux vectors of each inverter and the PCC rotate with the same frequency. Hence, even if the initial angle of the virtual flux vector of each inverter is unknown, without dependence on the changes of the angular difference, the frequency will not be changed. Moreover, the voltage amplitude of the PCC can be controlled by regulating the nominal amplitude of the inverter flux.

VI. Study Results

The proposed control strategy is evaluated by simulating the microgrid and control system in the Matlab/Simulink software. In addition, the results of the proposed AVFD control strategy are compared to conventional methods. Moreover, a laboratory experiment is conducted to validate the feasibility of the presented method.

A. Simulation Results

The microgrid consisting of three parallel three-phase inverter based-DGs connected through the tie-lines, as shown in Fig. 8, has been simulated in Matlab/Simulink. The parameters are listed in Table II. The line inductance and the filter inductance are modeled as L_{eq} [19]. Without loss of generality, it has been assumed that the DGs have the same ratings. The microgrid control scheme using the proposed AVFD control strategy is compared to the conventional VFD control method and also the conventional droop technique based on $P-\omega$ and $Q-V$ with virtual impedance (CD-VI). The delivered powers by DGs based on the conventional VFD control method, the conventional droop with virtual impedance and the proposed AVFD control strategy are respectively shown in Figs. 9-11. A step decrease and a step

This article has been accepted for publication in a future issue of this journal, but has not been fully edited. Content may change prior to final publication. Citation information: DOI 10.1109/JESTPE.2021.3108179, IEEE Journal of Emerging and Selected Topics in Power Electronics

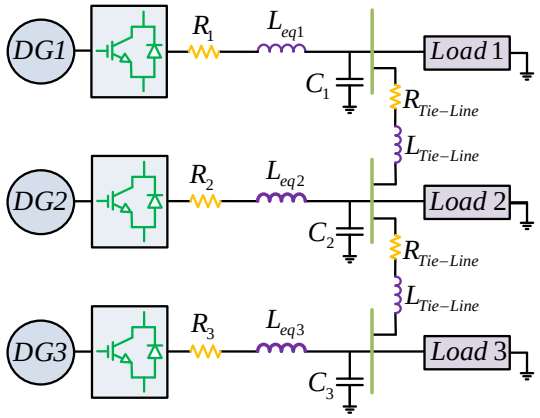

Fig. 8. Schematic diagram of the islanded microgrid under study.

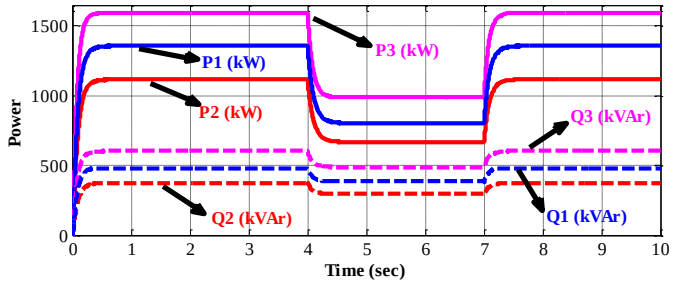

Fig. 9. Power sharing based on the conventional VFD method.

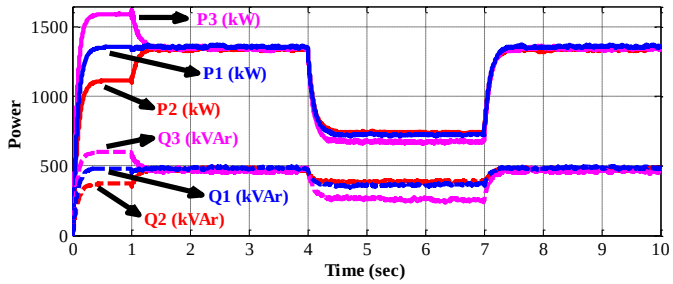

Fig. 10. Power sharing based on the CD-VI method.

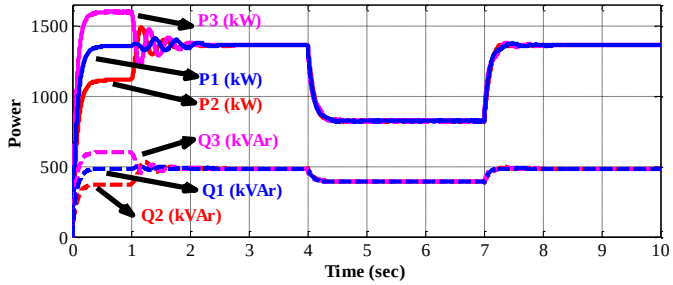

Fig. 11. Power sharing based on the proposed AVFD strategy.

increase of the total load power occur at t=4s and t=7s, respectively. Both the CD-VI method and the proposed AVFD control strategy are applied at t=1s. As can be seen in these figures, the conventional VFD control method leads to significant both active and reactive power mismatches between DGs. Although the conventional droop method with virtual impedance can reduce the power mismatches between the DGs, it is not effective enough and the power mismatches are not negligible and even increase when the demanded load power changes during t=4s and t=7s. But, the proposed AVFD control strategy can deal adequately with the line impedance mismatches which leads to appropriate power sharing between DGs despite the load changes during t=4s and t=7s, which shows the effectiveness of the proposed method.

Fig. 12 shows the injected currents by the DGs based on the conventional VFD control method, where improper current sharing between the DGs is visible. These current waveforms are different in phase and magnitude. Although enabling the CD-VI control method at t=1s can mitigate somewhat the phase and the magnitude differences between the injected current waveforms of DGs shown in Fig. 13, these differences are still significant and thus the performance of the CD-VI control method cannot meet the requirements. But, the injected currents of DGs become quite similar in phase and magnitude after activating the proposed AVFD control method at t=1s, as shown in Fig. 14. As a result, it represents a significant improvement in the accuracy of the current sharing.

Figs. 15 and 16 show the load-side voltages for the DGs based on the CD-VI control method and the proposed AVFD control strategy, respectively, which are enabled at t=1s. The voltage difference between bus 1 and bus 2 is negligible, but the voltage difference between bus 1 and bus 3 is about 100 V before t=1s. After enabling the CD-VI control method, it cannot show good performance in the voltage control of the microgrid. Therefore, the voltage differences between the load-side buses are still significant and also the voltage deviations are visible. By contrast, as a result of activating the

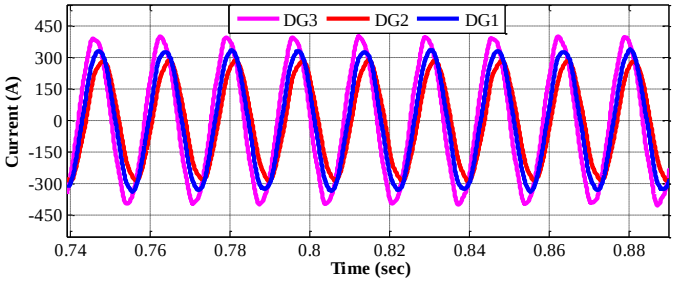

Fig. 12. Injected current to the PCC based on the conventional VFD method.

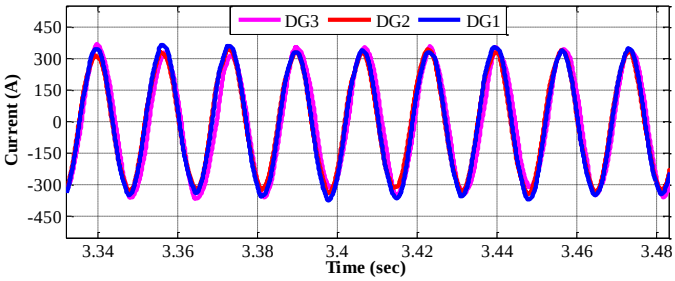

Fig. 13. Injected current to the PCC based on the CD-VI method.

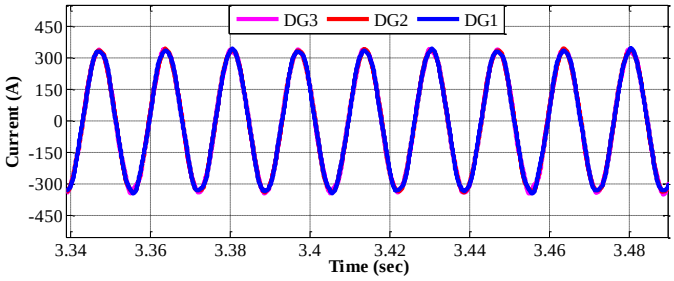

Fig. 14. Injected current to the PCC based on the proposed AVFD strategy.

This article has been accepted for publication in a future issue of this journal, but has not been fully edited. Content may change prior to final publication. Citation information: DOI 10.1109/JESTPE.2021.3108179, IEEE Journal of Emerging and Selected Topics in Power Electronics

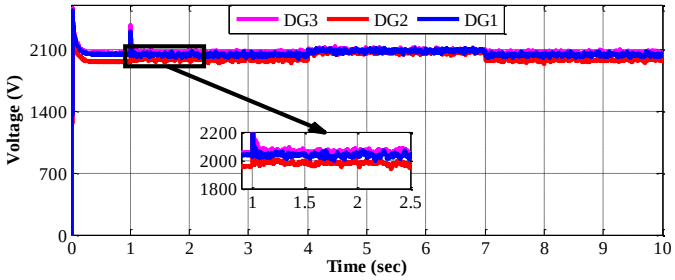

Fig. 15. Load-side voltages based on enabling the CD-VI method at t=1s.

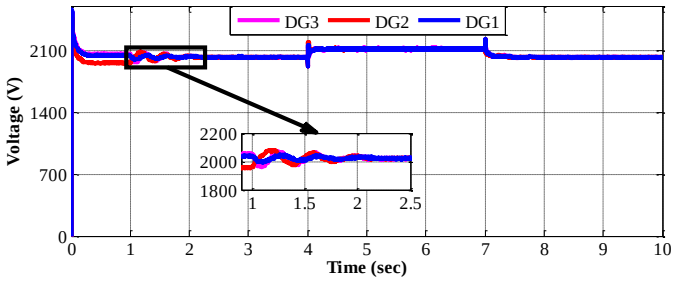

Fig. 16. Load-side voltages based on enabling the proposed AVFD strategy at t=1s.

proposed control strategy, the voltage differences between the load-side buses tend to zero and also the problem of voltage deviations does not emerge. In other words, regarding the issue that the last terms of (36) and (37) can produce the same effects as the supposed virtual impedances, the proposed AVFD strategy improves the voltage control of the PCC. As a result, the supposed virtual impedance is increased indirectly for the line with, smaller physical impedance. Similarly, it can happen vice-versa. Hence, the load-side voltages of the microgrid can be controlled correctly, which confirms the effectiveness of the proposed AVFD strategy.

Fig. 17 shows the PCC frequency of the microgrid. At t=1s, when the CD-VI and the proposed AVFD control methods are applied, fluctuations emerge during the transient state. However, the better frequency control based on angle droop employed by the VFD and the proposed AVFD control methods leads to that the magnitude of fluctuations is very smaller than the CD-VI method which uses $P-\omega$ droop. Moreover, the frequency deviations are fairly small in the conventional VFD and the proposed AVFD control methods in the steady-state. In addition, when the load changes at t=4s and t=7s, the magnitude of frequency fluctuations is not high. Therefore, the performance of the proposed method in frequency control is appropriate.

B. Performance Comparison

In this section, a quantitative performance assessment of the proposed AVFD control method in the condition of the unequal line impedances is provided in comparison to the conventional VFD control and also the CD-VI control methods. Based on the simulation analysis, the comparison results are reported in Table III. f_{err} and V_{err} are respectively magnitudes of the frequency and the voltage deviations in steady-state, THD_v and THD_c are respectively PCC voltage and delivered current THD indices. Moreover, the active

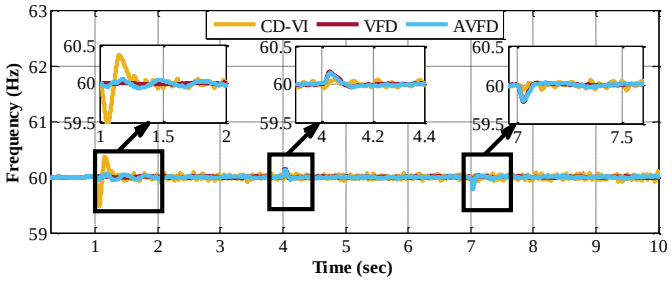

Fig.17. Microgrid frequency.

power the reactive power errors are calculated as:

$$Q_{err,i}=\frac{Q_i-Q_i^{\exp}}{Q_i^{\exp}}\times 100 \tag{60}$$

$$P_{err,i}=\frac{P_i-P_i^{\exp}}{P_i^{\exp}}\times 100 \tag{61}$$

where, P_i and Q_i are respectively the actual active power and the actual reactive power, $P_i^{\exp}$ and $Q_i^{\exp}$ are respectively the expected active power and the reactive power. Given that the DGs are assumed to have similar ratings, the active power and the reactive power delivered by DG1 are considered as the expected values.

According to Figs. 9-11, P_{err} and Q_{err} change when the total load decreases from the nominal value. As can be seen, the power sharing errors based on the conventional VFD control method are significant.

Performance of the CD-VI control method in the condition of the nominal load can be acceptable because the power sharing errors are about 2%. However, the errors (especially reactive power error) increase significantly when the total load changes. In contrary, the proposed AVFD control method shows an excellent performance in proportional power sharing, compared to the two other methods despite changing the total load. This proves the efficiency of the proposed AVFD control method. It should be noted that the values of P_{err} and Q_{err} in Table III are related to the condition of a step decrease of the total load occurs.

According to Figs. 12-16, the mismatched line impedances and consequently inappropriate power sharing lead to unequal line currents. Therefore, more current flows through the line with smaller equivalent inductance that results in the deterioration of THD indices. In addition, despite using the multiple feedback signals and the multi-loop structure, the CD-VI control method suffers from voltage and frequency deviations, and the control accuracy depends on the quality of the current control loop which uses PI regulators. The results comparison indicates that the THD indices in the CD-VI control method are greater than the virtual flux based control methods. Furthermore, In the structure of the proposed AVFD control method, the impacts of mismatched line impedances on the control parameters, i.e. $d\delta$ and $d\Psi$, are compensated, and therefore proportional power sharing is achieved. Furthermore, less frequency variation and better voltage and current control are also obtained which in-turn reduce THD indices.

C. Experimental Results

In order to validate the performance of the proposed control strategy, an islanded microgrid with parallel configuration, which consists of two inverter based-DGs with the same ratings, and its control system was made in the laboratory, as shown in Fig. 18. The parameters are listed in Table II. The primary sources for the inverters are supplied by two three-phase full-bridge rectifiers connected to the secondary of an autotransformer. The inverters use IRGP4069D IGBT modules. The proposed control method for inverters is carried out in Matlab/Simulink. The Matlab/Embedded Coder is employed to generate the usable code for Code Composer Studio Integrated Development Environment. The code is finally run on a TMS320F28335 32-bit floating-point DSP. This microcontroller contains six enhanced PWM modules (each one consists of two reversed PWM channels), which are used to send the switching commands to the IGBTs. Twelve analog-to-digital converter channels are used to provide inputs of the control strategy. The active and reactive powers are calculated internally by DSP and sent to the Host by SCI connection. The sampling frequency of the system is 10 kHz.

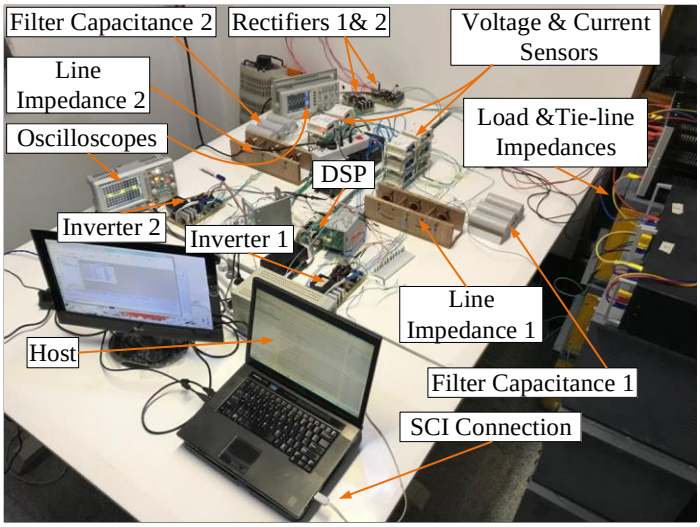

Fig. 18. Full experimental setup of the islanded microgrid.

TABLE II
PARAMETERS OF THE MICROGRID

Item	Symbol	Simulation	Experiment
Line Resistances	R_1,R_2,R_3	20, 40, 30 mΩ	40, 40 mΩ
Line Inductances	L_1,L_2,L_3	3,4.5, 1.5 mH	2, 4 mH
Tie- line Resistance	$R_{Tie\text{-}Line}$	75 mΩ	75 mΩ
Tie-line Inductance	$L_{Tie\text{-}Line}$	10 mH	10 mH
Filter Capacitance	C	120 µF	100 µF
Filter Inductance	L	4 mH	4 mH
Nominal Voltage	E^n	3500 V	155 V
Nominal Frequency	f	60 Hz	60 Hz
DGs Output Voltage	V_{dc}	10 kV	250 V
Nominal Flux Amplitude	$\lvert\psi^n\rvert$	7.8 Wb	0.42 Wb
Nominal Active Power	P^n	1400 kW	220 W
Nominal Reactive Power	Q^n	500 kVAr	145 VAr
Slope of $P-\delta$ Droop	m	-1.67×10^{-7} rad/W	-12×10^{-5} rad/W
Slope of $Q-\lvert\psi\rvert$ Droop	n	-1.65×10^{-6} Wb/Var	-4×10^{-5} Wb/VAr
Gain of k_q	k_q	12×10^{-5}	8×10^{-4}
Gain of k_p	k_p	1×10^{-5}	14×10^{-4}

TABLE III
COMPARISON BETWEEN THE PROPOSED AVFD METHOD AND THE CONVENTIONAL METHODS

Method	f_{err}	E_{err} %	$P_{err,1,2}$	$Q_{err,1,2}$	THD_v	THD_c
VFD	0.01	4.87	17.5, 17.8	25.4,22.6	3.23	2.55
CD-VI	0.05	3.75	25, 24,4	22.6, 23.2	3.39	4.63
AVFD	0.02	<1	-	-	2.08	1.70

In order to experimentally evaluate the operation of the proposed control method, three cases are considered. In case 1, the proposed AVFD control strategy is activated after the conventional VFD control method. In case 2, a step decrease in load occurs. Finally, in case 3 the load increases to the initial value by a step change. It is noteworthy to mention that 20 ms has been considered for the elapsed time during the process of receiving the references by control units of the DGs from EMS.

Case 1:

In order to compare the results, firstly, the power sharing is controlled by the conventional VFD method. Then, the proposed AVFD control strategy is applied at t=2s. The waveforms of the load-side voltages for both bus 1 and bus 2,

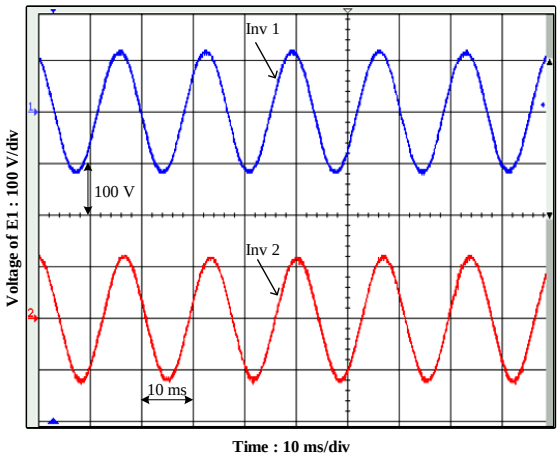

Fig. 19. Load-side voltage waveforms based on the conventional VFD control strategy for power sharing, captured from the laboratory test in case 1.

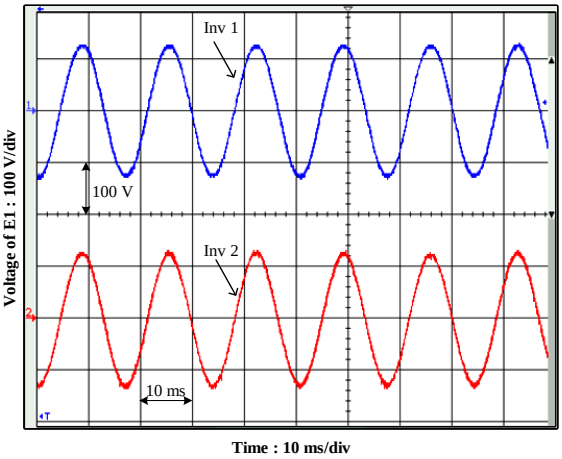

Fig. 20. Load-side voltage waveforms after applying the proposed AVFD control strategy for power sharing, captured from the laboratory test in case 1.

before and after applying the proposed AVFD control strategy are respectively shown in Figs. 19 and 20. As can be seen, the waveforms are quite sinusoidal. Moreover, the load-side voltages are similar in amplitude, which is about 125 V.

Figs. 21 and 22 show the injected currents of DGs, before and after enabling the proposed AVFD control strategy for power sharing. The current waveforms are firstly different in amplitude and phase. In addition, harmonics analysis has shown the THD index is equal to 4.08%. When the proposed AVFD control strategy is applied, the injected currents of DGs look quite similar in amplitude and phase. Also, it is found that the THD index for this case is 3.36%.

As mentioned earlier, the power data is captured from DSP by the SCI connection and plotted in the environment of Matlab/Simulink software as shown in Fig. 23. DG1 with lower line impedance delivers higher active and reactive powers while the conventional VFD control method is used for the power sharing, which leads to +10% error for the reactive power and +34% error for the active power. Moreover, the active and reactive power errors of DG2, which has higher line impedance, are -34% and -10%, respectively. After the proposed AVFD control strategy is activated, DG1 and DG2 become similar in the delivered active and reactive powers. This is primarily due to the effect of enabling the proposed AVFD control strategy for power sharing, which leads to an increase in the total impedance of the line with lower physical impedance and a decrease in the impedance of the line with higher physical impedance.

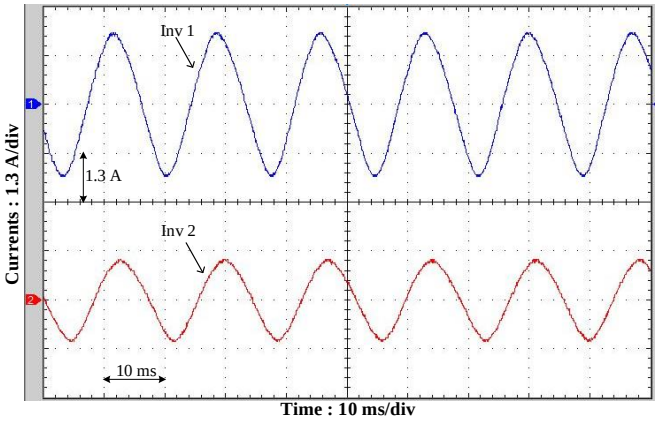

Fig. 21. Injected current waveforms to the PCC based on the VFD control strategy for power sharing, captured from the laboratory test in case 1.

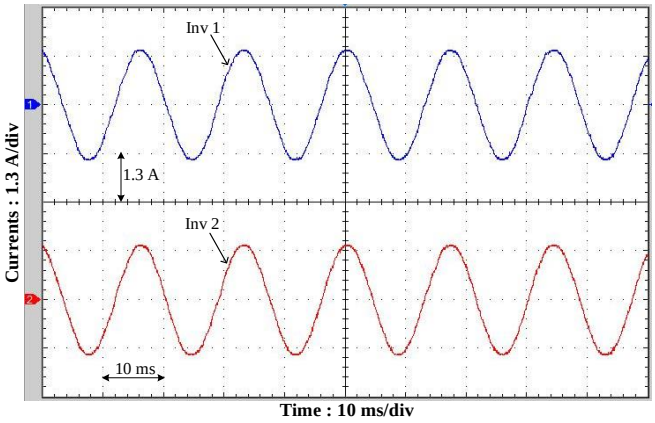

Fig. 22. Injected current waveforms after applying the proposed AVFD control strategy for power sharing, captured from the laboratory test in case 1.

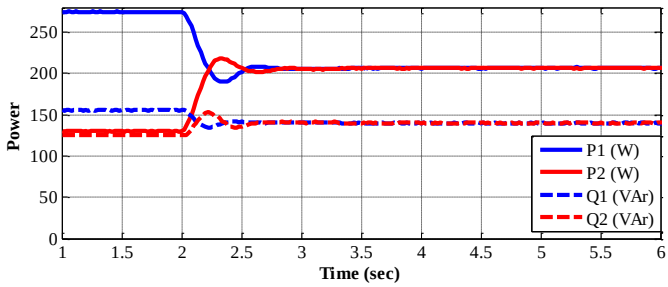

Fig. 23. Delivered powers to the PCC captured from the laboratory test in case 1.

Case 2:

In this case, a step decrease occurs in load. Fig. 24 shows the voltage waveforms. As can be seen, the changes are negligible. However, the voltages are increased slightly, due to the change in the voltage drop across the line impedances.

Fig. 25 shows the injected current waveforms of the DGs which are reduced because of the reduction in the load. Therefore, as shown in Fig. 26, the injected powers by DGs are decreased. As can be seen, the output active and reactive

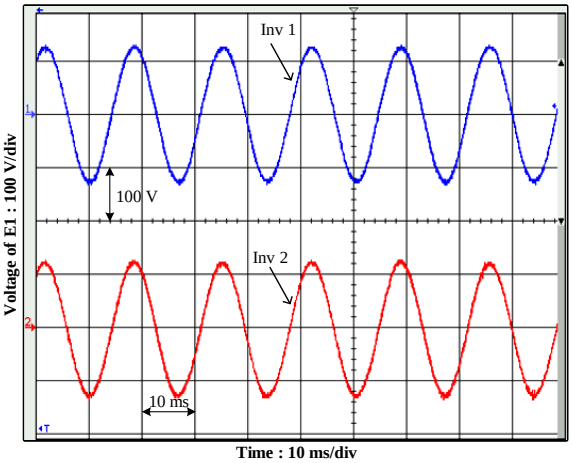

Fig. 24. Load-side voltage waveforms based on the proposed AVFD control strategy for power sharing, captured from the laboratory test in case 2.

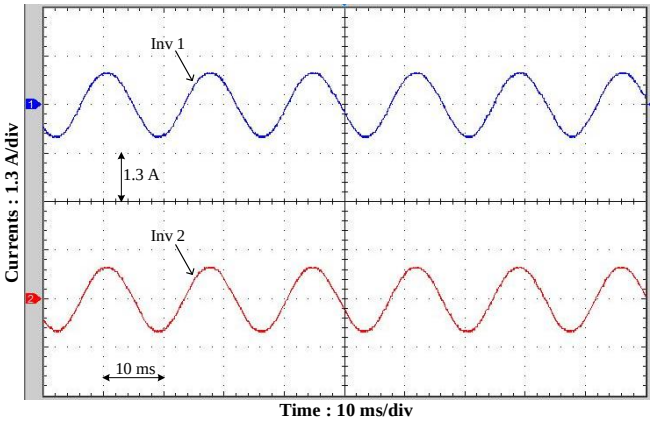

Fig. 25. Injected current waveforms to the PCC based on the proposed AVFD control strategy for power sharing, captured from the laboratory test in case 2.

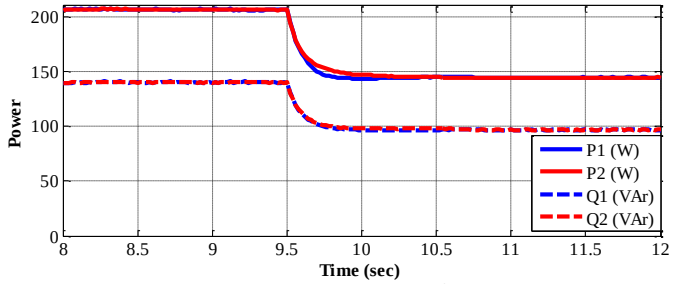

Fig. 26. Delivered powers to the PCC, captured from the laboratory test in case 2.

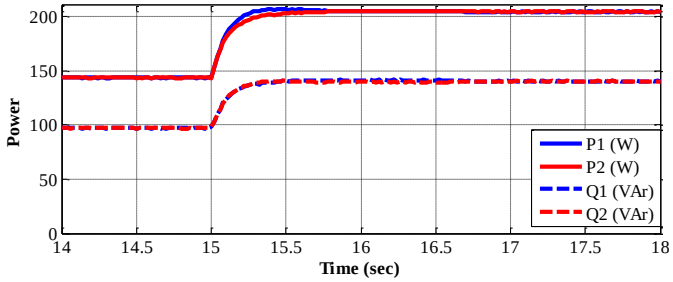

Fig. 27. Delivered powers to the PCC, captured from the laboratory test in case 3.

powers of the DGs are still similar in the new steady-state achieved after the step decrease occurs in load. In this situation, it is found that the THD index of the current waveforms is equal to 2.98%.

Case 3:

In this case, the total load demand reaches the initial value by a step increase. The output active and reactive powers of both DGs are shown in Fig. 27. It is observed that the injected powers are increased immediately to meet the new load demand. Subsequently, both DG1 and DG2 become similar in the output power when the system reaches the new steady-state, which shows the effectiveness of the proposed control strategy.

VII. Conclusion

Mismatched line impedances in the islanded AC microgrid with parallel configuration can result in active and reactive power sharing errors. An adaptive virtual flux droop control strategy has been proposed in this paper to solve this problem. In addition, the idea of virtual impedance has been employed to propose the control strategy. Moreover, in the microgrid control algorithm, the direct flux control technique has been used to generate the switching signals of the inverters based on the specified angular difference and the virtual flux amplitude of the inverter. Therefore, a simple control strategy is achieved without the need for complex transformations, multiple feedback control loops, knowledge of the line parameters and load data. The effectiveness and the feasibility of the proposed control strategy are verified by simulation and laboratory experiments. The corresponding results show that the proposed method can share active and reactive powers between the inverter-based DGs proportionally to their ratings despite unequal line impedances.

References

[1] F. Blaabjerg, Z. Chen, and S. B. Kjaer, "Power electronics as efficient interface in dispersed power generation systems," *IEEE Trans. Power Electron.*, vol. 19, no. 5, pp. 1184-1194, Sep. 2004

[2] Y. Han, H. Li, P. Shen, E. A. A. Coelho, and J. M. Guerrero, "Review of active and reactive power sharing strategies in hierarchical controlled microgrids," *IEEE Trans. Power Electron.*, vol. 32, no. 3, pp. 2427-2451, Mar. 2017.

[3] R. Razi, H. Iman-Eini and M. Hamzeh, "An impedance-power droop method for accurate power sharing in islanded resistive microgrids," *IEEE J. Emerg. Sel. Topics Power Electron.*, vol. 8, no. 4, pp. 3763-3771, Dec. 2020.

[4] Y. Li, Z. Zhang, C. Hu, M. Abdelrahem, R. Kennel and J. Rodriguez, "A full state-variable direct predictive control for islanded microgrids with parallel converters," *IEEE J. Emerg. Sel. Topics Power Electron.*, vol. 9, no. 4, pp. 4615-4628, Aug. 2021.

[5] J. Kim, J. M. Guerrero, P. Rodriguez, R. Teodorescu, and K. Nam, "Mode adaptive droop control with virtual output impedances for an inverter-based flexible AC microgrid," *IEEE Trans. Power Electron.*, vol. 26, no. 3, pp. 689-701, Mar. 2011.

[6] W. Cao, M. Han, X. Zhang, W. Xie, G. Agundis-Tinajero and J. M. Guerrero, "A novel power sharing scheme of controlling parallel-operated inverters in islanded microgrids," *IEEE J. Emerg. Sel. Topics Power Electron.*, 2020, (early access).

[7] T. V. Hoang and H. Lee, "An adaptive virtual impedance control scheme to eliminate the reactive-power-sharing errors in an islanding meshed microgrid," *IEEE J. Emerg. Sel. Topics Power Electron.*, vol. 6, no. 2, pp. 966-976, Jun. 2018.

[8] F. Zandi, B. Fani, I. Sadeghkhani and A. Orakzadeh, "Adaptive complex virtual impedance control scheme for accurate reactive power sharing of inverter interfaced autonomous microgrids," *IET Gener. Transmiss. Distrib.*, vol. 12, no. 22, pp. 6021-6032, Dec. 2018.

[9] J. M. Guerrero, J. Matas, L. G. de Vicuna, M. Castilla, and J. Miret, "Decentralized control for parallel operation of distributed generation inverters using resistive impedance," *IEEE Trans. Ind. Electron.*, vol. 54, no. 2, pp. 994–1004, Apr. 2007.

[10] J. M. Guerrero, L. G. de Vicuna, J. Matas, M. Castilla, and J. Miret, "Output impedance design of parallel-connected UPS inverters with wireless load-sharing control," *IEEE Trans. Ind. Electron.*, vol. 52, no. 4, pp. 1126–1135, Aug. 2005.

[11] W. Yao, J. Matas, J. M. Guerrero, and Z. –M. Qian, "Design and analysis of the droop control method for parallel inverters considering the impact of the complex impedance on the power sharing," *IEEE Trans. Ind. Electron.*, vol. 58, no. 2, pp. 576–588, Feb. 2011.

[12] Y. Chen, J. M. Guerrero, Z. Shuai, Z. Chen, L. Zhou, and A. Luo, "Fast reactive power sharing, circulating current and resonance suppression for parallel inverters using resistive-capacitive output impedance," *IEEE Trans. Power Electron.*, vol. 31, no. 8, pp. 5524-5537, Aug. 2016.

[13] Y. Zhu, F. Zhuo, F. Wang, B. Liu, and Y. Zhao, "A wireless load Sharing strategy for islanded microgrid based on feeder current sensing," *IEEE Trans. Power Electron.*, vol. 30, no. 12, pp. 6706-6719, Dec. 2015.

[14] Z. Peng, J. Wang, D. Bi, Y. Wen, Y. Dai, X. Yin, and Z. J. Shen, "Droop control strategy incorporating coupling compensation and virtual impedance for microgrid application," *IEEE. Trans. Energy Conv.*, vol. 34, no. 1, pp. 277-291, Mar. 2019.

[15] H. Mahmood, D. Michaelson, and J. Jiang, "Accurate reactive power sharing in an islanded microgrid using adaptive virtual impedances," *IEEE Trans. Power Electron.*, vol. 30, no. 3, pp. 1605-1617, Mar. 2015.

[16] D. M. Pham and H. Lee, "Effective coordinated virtual impedance control for accurate power sharing in islanded microgrid," *IEEE Trans. Ind. Electron.*, vol. 68, no. 3, pp. 2279-2288, Mar. 2021.

[17] H. Mahmood, D. Michaelson, and J. Jiang, "Reactive power sharing in islanded microgrids using adaptive voltage droop control," *IEEE Trans. Smart Grid.*, vol. 6, no. 6, pp. 3052-3060, Nov. 2015.

[18] R. Heydari, T. Dragicevic, and F. Blaabjerg, "High-bandwidth secondary voltage and frequency control of VSC-based AC microgrid," *IEEE Trans. Power Electron.*, vol. 34, no. 11, pp. 11320-11331, Nov. 2019.

[19] J. Hu, J. Zhu, D. G. Dorrell, and J. M. Guerrero, "Virtual flux droop method—A new control strategy of inverters in microgrids," *IEEE Trans. Power Electron.*, vol. 29, no. 9, pp. 4704-47011, Sep. 2014.

[20] S. Khanabdal, M. Banejad, F. Blaabjerg, and N. Hosseinzadeh, "Virtual flux droop control with constant switching frequency for power sharing between parallel inverters in islanded microgrids," *27th Iranian Conference on Electrical Engineering (ICEE)*, Yazd, Iran, 2019, pp. 868-874.

[21] R. Majumder, G. Ledwich, A. Ghosh, S. Chakrabarti, and F. Zare "Droop control of converter-interfaced microsources in rural distributed generation," *IEEE Trans. Power Del.*, vol. 25, no. 4, pp. 2768–2778, Oct. 2010.

[22] Y. Sun, X. Hou, J. Yang, H. Han, M. Su, and J. M. Guerrero, "New perspectives on droop control in AC microgrid," *IEEE Trans. Ind. Electron.*, vol. 64, no. 7, pp. 5741-5745, Jul. 2017.

[23] K. Ogata, Modern Control Engineering, 5ed, Prentice Hall, 2010, pp. 164-179.

Saheb Khanabdal received the B.Sc. degree from K.N. Toosi University of Technology, Tehran, Iran, in 2011 and the M.Sc. degree from University of Tabriz, Tabriz, Iran in 2013, both in electrical engineering. He is currently working toward the Ph.D. degree with the Faculty of Electrical Engineering, Shahrood University of Technology, Shahrood, Iran.

From June 2018 to September 2018, he was with Sustainable Energy Research Center at SQU, as a research assistant in Muscat, Oman. His current research interests include control of microgrid and power converters, electric vehicles, and fault current limiters.

Mahdi Banejad (SM'15) received the Ph.D. degree in electrical engineering from the Queensland University of Technology, Brisbane, QLD, Australia, in 2004.

He is currently an Associate Professor with the Faculty of Electrical Engineering, Shahrood University of Technology, Shahrood, Iran. His main research interests include distribution expansion planning, droop-based voltage and frequency control of microgrids, decentralized state estimation in the distribution system, and small-signal stability of microgrids. He was also visiting scholar at QUT, Australia (2014 and 2017), at Aalborg university, Denmark (2016) and at SQU, Oman (2018).

Frede Blaabjerg (S'86–M'88–SM'97–F'03) was with ABB-Scandia, Randers, Denmark, from 1987 to 1988. From 1988 to 1992, he got the Ph.D. degree in Electrical Engineering at Aalborg University in 1995. He became an Assistant Professor in 1992, an Associate Professor in 1996, and a Full Professor of power electronics and drives in 1998. From 2017 he became a Villum Investigator. He is honoris causa at University Politehnica Timisoara (UPT), Romania and Tallinn Technical University (TTU) in Estonia.

His current research interests include power electronics and its applications such as in wind turbines, PV systems, reliability, harmonics and adjustable speed drives. He has published more than 600 journal papers in the fields of power electronics and its applications. He is the co-author of four monographs and editor of ten books in power electronics and its applications.

He has received 33 IEEE Prize Paper Awards, the IEEE PELS Distinguished Service Award in 2009, the EPE-PEMC Council Award in 2010, the IEEE William E. Newell Power Electronics Award 2014, the Villum Kann Rasmussen Research Award 2014, the Global Energy Prize in 2019 and the 2020 IEEE Edison Medal. He was the Editor-in-Chief of the IEEE Transactions on Power Electronics from 2006 to 2012. He has been Distinguished Lecturer for the IEEE Power Electronics Society from 2005 to 2007 and for the IEEE Industry Applications Society from 2010 to 2011 as well as 2017 to 2018. In 2019-2020 he served as a President of IEEE Power Electronics Society. He has been Vice-President of the Danish Academy of Technical Sciences.

He is nominated in 2014-2020 by Thomson Reuters to be between the most 250 cited researchers in Engineering in the world.

Nasser Hosseinzadeh (SM'11) received his Ph.D. degree in electrical power systems from Victoria University in Australia in 1998; Earlier, he had received a B.Sc. degree from Shiraz University and an M.Sc. degree from Iran University of Science and Technology. He worked at Shiraz University from 1998 to 2002, at Monash University Malaysia from 2002 to 2003, at CQuniversity Australia from 2003 to 2008, at Swinburne University Australia from 2008 to 2011, at SQU Oman from 2011 to 2019, and is currently with Deakin University Australia, where he is the Director of the Centre for Smart Power and Energy Research (cSPER). Previously, he was the Discipline Leader of Electrical Engineering from 2005 to 2006 and the Head of Department of Systems from 2007 to 2008 at CQuniversity, and Head of Electrical and Computer Engineering at SQU Oman from 2014 to 2018.

Nasser's research interests include stability assessment of the power grid as impacted by new types of distributed generators and microgrids; power system dynamics and control; on-line monitoring and real-time control of microgrids and virtual power plants. He has been a regular reviewer for the IEEE Transactions on Smart Grid, IEEE Transactions on Power Systems, IEEE Transactions on Power Delivery, IEEE Transactions on Neural Networks and Learning Systems, IEEE Transactions on Education, and International Journal of Electrical Power and Energy Systems.